Materials Science Forum
ISSN: 1662-9752, Vol. 1093, pp 73-86
doi:10.4028/p-cmRyy7

Submitted: 2022-07-03
Revised: 2022-12-15
Accepted: 2023-01-04
Online: 2023-07-21

Electrical Properties of Heavily Al-Doped 4H-SiC

Hideharu Matsuura[a*], Akinobu Takeshita[b], Rinya Nishihata[c], Yuuki Kondo[d], and Atsuki Hidaka[e]

Department of Electrical and Electronic Engineering, Osaka Electro-Communication University, Neyagawa, Osaka 572-8530, Japan

[a]matsuura@osakac.ac.jp, [b]mf15a004@oecu.jp, [c]ee14a060@oecu.jp, [d]mf20a005@oecu.jp, [e]h-atsuki@osakac.ac.jp

Keywords: p-Type 4H-SiC, Heavily Al-Doped 4H-SiC, Resistivity, Hall Coefficient, Sign of Hall Coefficient, Hopping Conduction, Activation Energy

Abstract. We investigate the temperature-dependent resistivity ($\rho(T)$) and Hall coefficient ($R_{\mathrm{H}}(T)$) of heavily Al-doped 4H-SiC and discuss the underlying conduction mechanisms. The sign of $R_{\mathrm{H}}(T)$ changes from positive to negative in nearest-neighbor hopping (NNH) and variable-range hopping (VRH) conduction, whereas it is positive in band conduction because Al-doped 4H-SiC is a p-type semiconductor. We propose a general physical model to explain why $R_{\mathrm{H}}(T)$ in hopping conduction becomes negative at low temperatures, which is applicable to both NNH and VRH conduction. Moreover, we elucidate why the activation energy for negative $R_{\mathrm{H}}(T)$ becomes similar to that of $\rho(T)$ in NNH conduction.

Introduction

In power semiconductor devices, it is crucial to reduce energy losses, even in low-resistivity layers such as the thick p-type collector layers of n-channel insulated-gate bipolar transistors. For p-type SiC, however, the fabrication of heavily Al-doped substrates with very low resistivity is challenging [1, 2]. The literature contains numerous studies of the electrical transport properties of heavily Al-implanted 4H-SiC layers [3–7], Al-doped 4H-SiC epilayers grown by chemical vapor deposition (CVD) [8, 9], and Al-doped 6H-SiC wafers grown by physical vapor transport (PVT) [10, 11]. Our group has previously investigated the temperature-dependent resistivity ($\rho(T)$) and temperature-dependent Hall coefficient ($R_{\mathrm{H}}(T)$) for heavily Al-doped 4H-SiC epilayers grown via CVD, PVT, and a solution method [12–20]. In the case of CVD-grown samples, we characterized the relationships between the conduction mechanisms (i.e., band, nearest-neighbor hopping (NNH), and variable-range hopping (VRH) conduction) and both the measurement temperature (T) and the Al concentration (C_{Al}) [13].We found that, although the Al dopant makes 4H-SiC a p-type semiconductor, the value of $R_{\mathrm{H}}(T)$ for all of the samples became negative at low temperatures. We experimentally elucidated the relationship between the sign of $R_{\mathrm{H}}(T)$ and the band and NNH conduction regions [16,17] and found that the activation energies ($\Delta E_{\mathrm{RHBand}}$ and $\Delta R_{\mathrm{RHNNH}}$) associated with $R_{\mathrm{H}}(T)$ in band and NNH conduction, respectively, are similar to those ($\Delta E_{\rho\mathrm{Band}}$ and $\Delta E_{\rho\mathrm{NNH}}$, respectively) for the corresponding $\rho(T)$ [16,17].

In the case of p-type-conducting single-crystalline SiC, the sign of $R_{\mathrm{H}}(T)$ was found to become negative at low temperatures [3, 9, 10, 16–19]. In addition, the sign of $R_{\mathrm{H}}(T)$ has also been reported to become negative for Mg-doped InP [21], Mn-doped InP [22], and Mg-doped GaN [23] at low temperatures. In the case of Al-doped 6H-SiC, Krieger et al. [10] explained the negative $R_{\mathrm{H}}(T)$ in NNH conduction on the basis of the amorphous semiconductor models proposed by Emin [24], Grunewald et al. [25], Holstein [26], and Németh and Mühlschlegel [27], where they discussed the Hall effect for hopping conduction on a quantum theoretical basis (i.e., from the perspective of the wavefunction of electrons). However, Street [28] has argued that these models are applicable to narrow-bandgap materials or materials whose mobility edge is located at the center of the band, whereas conduction in hydrogenated amorphous silicon (a-Si:H) occurs near the band edge. The sign reversal of $R_{\mathrm{H}}(T)$

has been observed in a-Si:H, where the localized states are the dominant contributor to the resistivity. That is, positive and negative $R_{\rm H}(T)$ values have been reported for n- and p-type a-Si:H, respectively [29–31]. However, $R_{\rm H}(T)$ values with the expected sign were observed in microcrystalline Si with a grain size as small as $3-5$ nm [28, 32] and in a-Si:H in which extended states (i.e., delocalized states) were the dominant contributor to the resistivity [33]. Thus, under Street's argument, the aforementioned models are not applicable to Al-doped single-crystalline SiC, and the question of why $R_{\rm H}(T)$ for heavily-doped p-type crystalline semiconductors becomes negative remains unanswered. That is why we attempted to individually explain the sign of $R_{\rm H}(T)$ for NNH [18] and VRH [19] conduction using physical models developed from the perspective of electron and hole hopping.

In the present study, we rigorously investigate the conduction mechanisms for p-type 4H-SiC with $C_{\rm Al}$ greater than 2×10^{20} cm^{-3} and reconsider the relationships between the conduction mechanisms and the values of T and $C_{\rm Al}$. We then discuss the reason why the resistivity does not decrease with increasing $C_{\rm Al}$. We also propose a general physical model to explain the sign of $R_{\rm H}(T)$ for hopping conduction based on the viewpoint of electron and hole hopping. On the basis of the proposed model for $R_{\rm H}(T)$ in hopping conduction, finally, we discuss the density of charge carriers in NNH conduction, as determined by Hall effect measurements, which leads to an explanation for why the value of $\Delta E_{\rm RHNNH}$ becomes similar to the value of $\Delta E_{\rho\rm NNH}$.

Experimental

Al-doped 4H-SiC epilayers with a thickness of approximately 90 μm were grown using a horizontal hot-wall CVD system (VP508 GFR, Aixtron) at approximately 1620 °C on (0001)-oriented three-inch n$^+$-type 4H-SiC wafers (8° off-oriented toward $[11\bar{2}0]$) [1, 2, 12]. Four Al/Ti/Al contact dots in the van der Pauw configuration [34] were deposited by electron-beam evaporation of Al and Ti, and the samples were subsequently annealed at 1000 °C under a N_2 atmosphere. Eleven epilayers were prepared with $C_{\rm Al}$ values ranging from 2.4×10^{19} to 4.7×10^{20} cm^{-3}, as determined by secondary-ion mass spectrometry. Using a Hall effect measurement system (ResiTest8400, TOYO) in the temperature range of $20-600$ K, the $\rho(T)$ values for the samples were measured by the van der Pauw method, and their $R_{\rm H}(T)$ values were measured under an AC magnetic field of 0.35 T at a frequency of 0.1 Hz. The techniques used to obtain reliable $\rho(T)$ and $R_{\rm H}(T)$ values were described in our previous papers [14, 16]. The depletion layer formed by the p–n junction (i.e., a p-type epilayer/n$^+$-type substrate) has been confirmed to electrically isolate the p-type 4H-SiC epilayer from the n$^+$-type 4H-SiC substrate [18, 19], thereby enabling measurement of the electrical properties of the heavily Al-doped epilayer.

Results and Discussion

Conduction mechanisms. Figure 1 shows the dependence of the resistivity at 300 K on $C_{\rm Al}$. The resistivity for the samples with $C_{\rm Al}>2.4\times10^{20}$ cm^{-3} does not decrease with increasing $C_{\rm Al}$, whereas it does decrease for the samples with $C_{\rm Al}<2.4\times10^{20}$ cm^{-3}. Therefore, we discuss the relationship between the conduction mechanisms and $C_{\rm Al}$.

The conduction mechanisms in semiconductors include band conduction, NNH conduction [35], and VRH conduction [35]. Figure 2(a) and (b) show the density-of-states distribution and the energy band diagram near the top of the valence band ($E_{\rm V}$), respectively, for Al-doped 4H-SiC. Here, $N(E)$ represents the density of delocalized states in the valence band and $g(E)$ represents the density of localized states in the bandgap above $E_{\rm V}$, which is referred to as the band tail. At low $C_{\rm Al}$, only the holes in the valence band can flow, which corresponds to band conduction because the distance between nearest-neighbor Al acceptor sites is too great for holes at Al acceptor sites to hop to their nearest-neighbor Al acceptor sites. By contrast, at high $C_{\rm Al}$, holes at Al acceptor sites can hop to their nearest-neighbor unoccupied Al acceptor sites because of the shorter distance between Al acceptor

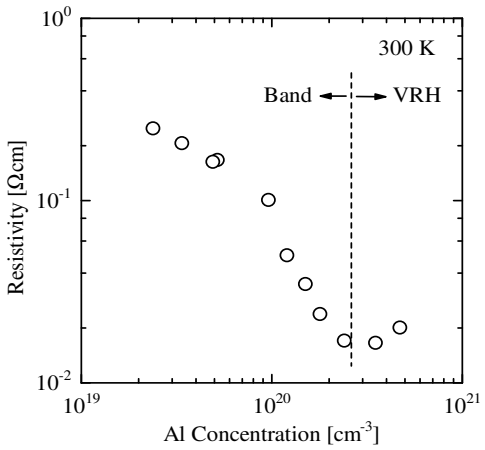

Fig. 1: Dependence of resistivity at 300 K on C_{Al}.

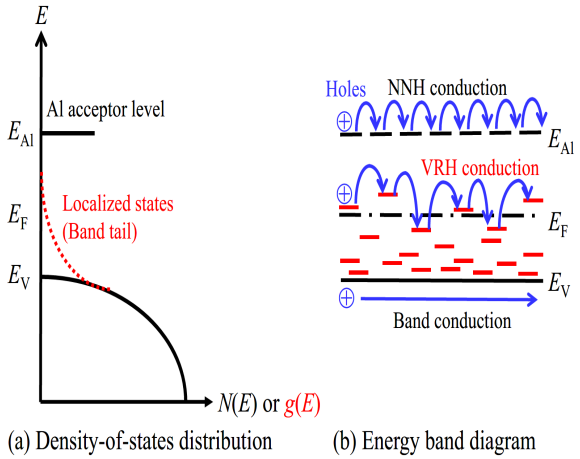

Fig. 2: (a) Density-of-states distribution and (b) energy band diagram for Al-doped 4H-SiC.

sites, leading to NNH conduction. At very high Al doping levels, local lattice distortion is speculated to increase because the covalent radius of a substitutional Al atom (0.125 nm) is larger than that of a Si atom (0.117 nm) [1], which can lead to a local disturbance of the lattice periodicity [15]. This periodicity disturbance indicates that band tails above E_{V} and below the bottom of the conduction band (E_{C}) must have formed. Because the Fermi level (E_{F}) has been reported to be located between E_{V} and the Al acceptor level (E_{Al}) even at high temperatures in the case of heavily Al-doped 4H-SiC [36,37], localized states must exist around E_{F}, as depicted in Fig. 2.

Figure 2(b) illustrates band conduction, in which holes flow in the valence band, NNH conduction, in which holes at Al acceptor sites hop to their nearest-neighbor unoccupied Al sites, and VRH conduction, in which holes at localized states around E_{F} hop to the most easily accessible unoccupied localized states around E_{F}. In the case where the currents due to band, NNH, and VRH conduction flow completely in parallel in the valence band, at E_{Al}, and around E_{F}, respectively, $\rho(T)$ can be expressed as

$$\frac{1}{\rho(T)} = \frac{1}{\rho_{\mathrm{Band}}(T)} + \frac{1}{\rho_{\mathrm{NNH}}(T)} + \frac{1}{\rho_{\mathrm{VRH}}(T)}, \tag{1}$$

where

$$\rho_{\mathrm{Band}}(T) = \rho_{0\mathrm{Band}} \exp\left(\frac{\Delta E_{\rho\mathrm{Band}}}{k_{\mathrm{B}}T}\right), \tag{2}$$

$$\rho_{\mathrm{NNH}}(T) = \rho_{0\mathrm{NNH}} \exp\left(\frac{\Delta E_{\rho\mathrm{NNH}}}{k_{\mathrm{B}}T}\right), \tag{3}$$

and

$$\rho_{\mathrm{VRH}}(T) = \rho_{0\mathrm{VRH}} \exp\left[\left(\frac{T_0}{T}\right)^{1/4}\right]. \tag{4}$$

Here, $\rho_{\mathrm{Band}}(T)$, $\rho_{\mathrm{NNH}}(T)$, and $\rho_{\mathrm{VRH}}(T)$ denote the temperature-dependent resistivities for band, NNH, and VRH conduction, respectively; $\rho_{0\mathrm{Band}}$, $\rho_{0\mathrm{NNH}}$, and $\rho_{0\mathrm{VRH}}$ are the pre-exponential factors for band, NNH, and VRH conduction, respectively; T_0 is a constant associated with VRH conduction; and k_{B} is the Boltzmann constant. Equation 1 shows that the lowest resistivity among the three conduction mechanisms becomes dominant at a given T. At high temperatures, band conduction is dominant because the hole concentration ($p(T)$) in the valence band becomes large. By contrast, at low temperatures, hopping conduction becomes dominant because $p(T)$ becomes very low.

Temperature dependences of the resistivity and Hall coefficient. Figure 3 shows plots of $\ln \rho(T)$ and $\ln |R_{\mathrm{H}}(T)|$ versus $1/T$ on the same vertical scale for the sample with a C_{Al} of 9.6×10^{19} cm^{-3}.

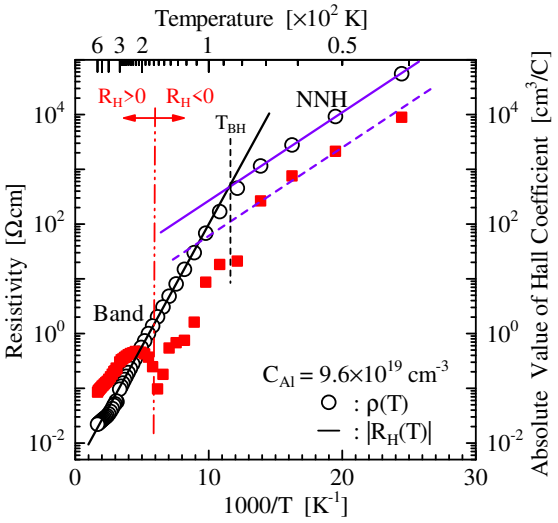

Fig. 3: Plots of $\ln \rho(T)$ and $\ln |R_{\mathrm{H}}(T)|$ versus $1/T$ for the sample with a C_{Al} of 9.6×10^{19}.

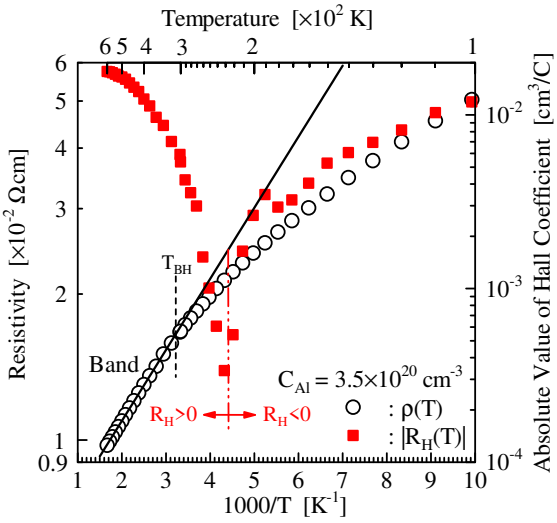

Fig. 4: Plots of $\ln \rho(T)$ and $\ln |R_{\mathrm{H}}(T)|$ versus $1/T$ for the sample with a C_{Al} of 3.5×10^{20} cm^{-3}.

The data in the $\ln \rho(T)$ versus $1/T$ plot are best approximated by two straight lines, indicating that, from Eqs. 2 and 3, the dominant conduction mechanisms at high and low temperatures are band and NNH conduction, respectively. The temperature at the point of intersection of the two solid straight lines extrapolated from the higher- and lower-temperature regions is denoted T_{BH}, the value of which is 85 K for the sample with a C_{Al} of 9.6×10^{19} cm^{-3}.

In Fig. 3, $R_{\mathrm{H}}(T)$ becomes negative for NNH conduction. The broken straight line for negative $R_{\mathrm{H}}(T)$ is drawn using the same slope of $\rho(T)$, indicating that in NNH conduction $\Delta E_{\mathrm{RHNNH}}$ is very close to $\Delta E_{\rho\mathrm{NNH}}$. The findings of negative $R_{\mathrm{H}}(T)$ for NNH conduction and $\Delta E_{\mathrm{RHNNH}} \simeq \Delta E_{\rho\mathrm{NNH}}$ are observed for the samples with $C_{\mathrm{Al}} \leq 1.5 \times 10^{20}$ cm^{-3}.

Figure 4 shows plots of $\ln \rho(T)$ and $\ln |R_{\mathrm{H}}(T)|$ versus $1/T$ for the sample with a C_{Al} of 3.5×10^{20} cm^{-3}. The data in the $\ln \rho(T)$ versus $1/T$ plot at high temperatures are best approximated by a straight line, indicating that the dominant conduction mechanism at high temperatures is band conduction. The data in the plot at low temperatures, however, cannot be approximated by a straight line. The value of T_{BH} is approximately 320 K, which is estimated to be the lowest temperature at which the data obey Eq. 2.

Figure 5 shows plots of $\ln \rho(T)$ and $\ln |R_{\mathrm{H}}(T)|$ versus $T^{-1/4}$ for the epilayer with a C_{Al} of 3.5×10^{20} cm^{-3}. The data in the $\ln \rho(T)$ versus $T^{-1/4}$ plot are best approximated by a straight line, which, according to Eq. 4, indicates that the dominant conduction mechanism at low temperatures is VRH conduction. At low temperatures in the VRH conduction region, $R_{\mathrm{H}}(T)$ is negative for the samples with $C_{\mathrm{Al}} \geq 1.8 \times 10^{20}$ cm^{-3}.

Figure 6 shows the relationship between the conduction mechanisms and the values of T and C_{Al}. For the epilayers with $C_{\mathrm{Al}} \geq 1.8 \times 10^{20}$ cm^{-3}, the dominant conduction mechanism is band conduction at high temperatures and NNH conduction at low temperatures. For the epilayers with C_{Al} values of 2.4×10^{19} and 3.4×10^{19} cm^{-3}, an unexpected conduction mechanism, referred to here as X conduction, appears between the band and NNH conduction regions [13, 20].

For the samples with $C_{\mathrm{Al}} > 2.4 \times 10^{20}$ cm^{-3}, the dominant conduction mechanism at room temperature is found to be VRH conduction, which originates from a local disturbance of the lattice periodicity due to the high degree of Al doping. This indicates that in VRH conduction the resistivity does not decrease with increasing C_{Al}, whereas it decreases in band conduction.

Hall coefficient. We consider three types of Hall coefficients: $R_{\mathrm{HBand}}(T)$, $R_{\mathrm{HNNH}}(T)$, and $R_{\mathrm{HVRH}}(T)$, corresponding to band, NNH, and VRH conduction, respectively. Figure 7(a) and (b) show the con-

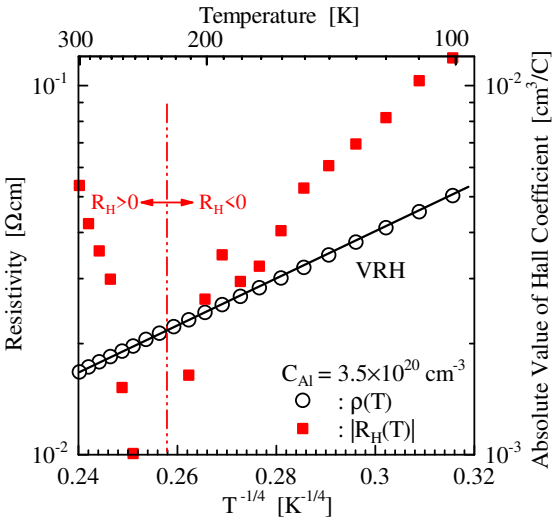

Fig. 5: Plots of $\ln \rho(T)$ and $\ln |R_{\mathrm{H}}(T)|$ versus $T^{-1/4}$ for the sample with a C_{Al} of 3.5×10^{20} cm^{-3}.

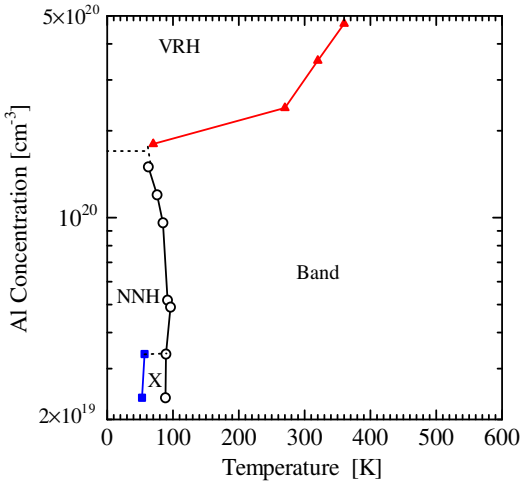

Fig. 6: Relationship between conduction mechanisms and values of T and C_{Al} in 4H-SiC epilayers.

figuration of the Hall measurement system and the equivalent circuit for the measured Hall voltage ($V_{\mathrm{H}}(T)$), respectively, where w is the thickness of the sample and four electrodes (electrodes 1 to 4) are positioned at the four corners of the sample. Here, B is the applied magnetic flux density; $V_{\mathrm{HBand}}(T)$, $V_{\mathrm{HNNH}}(T)$, and $V_{\mathrm{HVRH}}(T)$ are the Hall voltages corresponding to band, NNH, and VRH conduction, respectively; and $r_{\mathrm{Band}}(T)$, $r_{\mathrm{NNH}}(T)$, and $r_{\mathrm{VRH}}(T)$ are the resistances between electrodes 2 and 4 for band, NNH, and VRH conduction, respectively. The applied current (I) flowing from electrode 1 to electrode 3 is expressed as

$$I = I_{\mathrm{Band}} + I_{\mathrm{NNH}} + I_{\mathrm{VRH}}, \tag{5}$$

where I_{Band}, I_{NNH}, and I_{VRH} are the currents due to band, NNH, and VRH conduction, respectively.

$V_{\mathrm{H}}(T)$ and $V_{\mathrm{HBand}}(T)$ are respectively expressed as

$$V_{\mathrm{H}}(T) = R_{\mathrm{H}}(T)\frac{IB}{w} \tag{6}$$

and

$$V_{\mathrm{HBand}}(T) = R_{\mathrm{HBand}}(T)\frac{I_{\mathrm{Band}}B}{w}. \tag{7}$$

Analogous to $V_{\mathrm{HBand}}(T)$, $V_{\mathrm{HNNH}}(T)$ and $V_{\mathrm{HVRH}}(T)$ are defined as

$$V_{\mathrm{HNNH}}(T) \equiv R_{\mathrm{HNNH}}(T)\frac{I_{\mathrm{NNH}}B}{w} \tag{8}$$

and

$$V_{\mathrm{HVRH}}(T) \equiv R_{\mathrm{HVRH}}(T)\frac{I_{\mathrm{VRH}}B}{w}, \tag{9}$$

respectively. From the equivalent circuit diagram in Fig. 7(b), $R_{\mathrm{H}}(T)$ can be derived as [17, 18]

$$R_{\mathrm{H}}(T) = \left[\frac{\rho(T)}{\rho_{\mathrm{Band}}(T)}\right]^2 R_{\mathrm{HBand}}(T) + \left[\frac{\rho(T)}{\rho_{\mathrm{NNH}}(T)}\right]^2 R_{\mathrm{HNNH}}(T) + \left[\frac{\rho(T)}{\rho_{\mathrm{VRH}}(T)}\right]^2 R_{\mathrm{HVRH}}(T). \tag{10}$$

As evident from Figs. 3–5 and Eq. 10, $R_{\mathrm{HNNH}}(T)$ and $R_{\mathrm{HVRH}}(T)$ should be negative. Therefore, we discuss the sign of $R_{\mathrm{H}}(T)$ in hopping conduction.

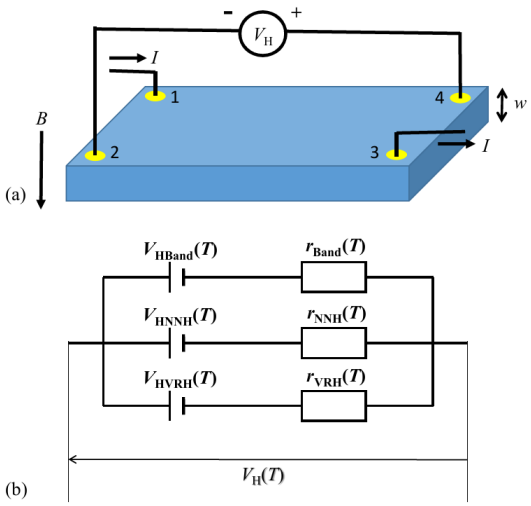

Fig. 7: Schematic diagrams of (a) the configuration of the Hall measurement system and (b) the equivalent circuit for the measured Hall voltage.

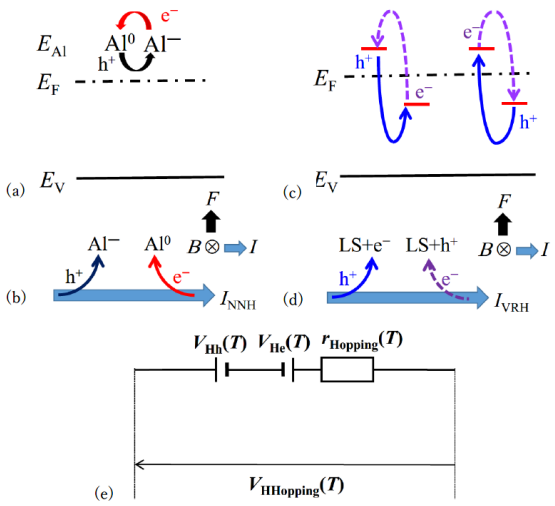

Fig. 8: Schematic diagrams of NNH and VRH conduction, and equivalent circuit for the Hall voltage due to hopping (NNH or VRH) current.

General physical model for the sign of $R_{\mathrm{H}}(T)$ in hopping conduction. Figure 8 shows schematic diagrams of NNH and VRH conduction under an electric field ($\mathcal{E}$) and B. Panels (a) and (b) depict the hopping of a hole or an electron for NNH conduction under $\mathcal{E}$ in an energy band diagram and under B in real space, respectively. The inset shows the hopping direction of the charge carriers, i.e., the force (F) affecting the flowing charge carriers, for left-to-right flowing current (I) with B directed toward the rear of the plane. Panels (c) and (d) show hole or electron hopping for VRH conduction under $\mathcal{E}$ in an energy band diagram and under B in real space, respectively. Although the phenomena illustrated in Fig. 8(b) and (d) can be described by classical physics, the direction of highest transfer probability for charge carriers under B, which is quantum-theoretically derived, has been reported to coincide with the direction indicated by the Lorentz force [38].

Under $\mathcal{E}$, in general, an electron hops from a bandgap state (e.g., acceptor, donor, and localized state) to another bandgap state unoccupied by an electron. Analogous to the concept of holes in the valence band, the bandgap state unoccupied by an electron can be regarded as the bandgap state occupied by a hole. Therefore, the hopping of holes is the same phenomenon as the hopping of electrons, and the hopping directions are opposite to each other, as depicted in Fig. 8(a) and (c), indicating that the mathematical representation for the hopping probability of holes between two bandgap states is the same as that of electrons. Consequently, the current in hopping conduction can be explained not only by the hopping of electrons from bandgap states to other bandgap states unoccupied by electrons but also by the hopping of holes from bandgap states to other bandgap states unoccupied by holes, as shown in Fig. 2(b). Because the density of hopping holes is the same as that of hopping electrons under $\mathcal{E}$, the net density of hopping charge carriers is referred to as $n_{\mathrm{Hopping}}(T)$.

In the following, we discuss the sign of $R_{\mathrm{H}}(T)$ from the perspective of the hopping of electrons and holes. For a left-to-right hopping current (I_{Hopping}), holes and electrons (of which n_{Hopping} consists) transfer in the upward direction under B directed toward the back of the plane, which results in a change of the charged state of the upper localized sites. In the case where the charged state becomes negative, which is defined as the hopping of electrons under B, this change in the charged state contributes to a negative Hall voltage. In the opposite case, which is defined as the hopping of holes under B, the change in the charged state contributes to a positive Hall voltage. These results indicate that the sign of $R_{\mathrm{H}}(T)$ depends on the change of the charged state of hopping sites under B.

Figure 8(e) shows the equivalent circuit for the measured Hall voltage due to hopping conduction ($V_{\mathrm{HHopping}}(T)$), where $V_{\mathrm{Hh}}(T)$ and $V_{\mathrm{He}}(T)$ are the Hall voltages due to the hopping of holes and

electrons, respectively, under B and $r_{\text{Hopping}}(T)$ is the resistance between electrodes 2 and 4 due to hopping conduction in Fig 7.

Assuming that holes or electrons, of which $n_{\text{Hopping}}(T)$ consists entirely, can hop under B, the absolute value of the ideal Hall voltage due to hopping conduction ($V_{\text{H0Hopping}}(T)$) is defined as [38]

$$V_{\text{H0Hopping}}(T) \equiv R_{\text{H0Hopping}}(T)\frac{I_{\text{Hopping}}B}{w}, \tag{11}$$

where $R_{\text{H0Hopping}}(T)$ is the absolute value of the ideal Hall coefficient for hopping conduction. This is determined by

$$R_{\text{H0Hopping}}(T) = \frac{\gamma_{\text{Hopping}}}{qn_{\text{Hopping}}(T)}, \tag{12}$$

where q is the elementary charge and γ_{Hopping} is the Hall factor for hopping conduction.

Because B affects hopping charge carriers whose density is n_{Hopping}, the ratio between the hopping probability of holes ($P_{\text{h}}(T)$) and the hopping probability of electrons ($P_{\text{e}}(T)$) due to B is the ratio between the density of hopping sites for holes and the density of hopping sites for electrons under B. Here,

$$P_{\text{h}}(T) + P_{\text{e}}(T) = 1. \tag{13}$$

The ratio between the amount of holes and the amount of electrons that accumulate at electrode 4 in Fig. 7(a) when B is applied is the ratio between $P_{\text{h}}(T)$ and $P_{\text{e}}(T)$. Because the internal resistance in the electronic voltmeter is too high for the current to flow, the voltage drop at $r_{\text{Hopping}}(T)$ in Fig. 8(e) is nearly equal to 0 V. Therefore, the ratio between $V_{\text{Hh}}(T)$ and $V_{\text{He}}(T)$ in Fig. 8(e) becomes the ratio between $P_{\text{h}}(T)$ and $P_{\text{e}}(T)$;

$$V_{\text{Hh}}(T) = V_{\text{H0Hopping}}(T)P_{\text{h}}(T) \tag{14}$$

and

$$V_{\text{He}}(T) = V_{\text{H0Hopping}}(T)P_{\text{e}}(T). \tag{15}$$

Consequently, $V_{\text{HHopping}}(T)$ can be expressed as

$$V_{\text{HHopping}}(T) = V_{\text{Hh}}(T) - V_{\text{He}}(T) = V_{\text{H0Hopping}}(T)\left[P_{\text{h}}(T) - P_{\text{e}}(T)\right], \tag{16}$$

the physical implication of which is the recombination of the holes and electrons accumulated at electrode 4.

In hopping conduction, electrons or holes are restricted to seeking unoccupied sites to hop to, indicating that the sign of $R_{\text{H}}(T)$ is determined by the difference between the density of hopping sites for holes and the density of hopping sites for electrons under B. That is, the sign of $R_{\text{H}}(T)$ becomes negative when the density of sites to which electrons can hop under B is greater than the density of hopping sites for holes. Conversely, the sign of $R_{\text{H}}(T)$ becomes positive when the density of sites to which holes can hop under B is greater than the density of hopping sites for electrons.

Sign of $R_{\text{H}}(T)$ in NNH conduction. In NNH conduction, as shown in Fig. 8(a), under $\mathcal{E}$ an electron hops from a negatively ionized Al acceptor (Al^-) site to its nearest-neighbor neutral Al acceptor (Al^0) site or a hole hops from an Al^0 site to its nearest-neighbor Al^- site.

In Fig. 8(e), $V_{\text{HHopping}}(T)$ and $r_{\text{Hopping}}(T)$ are replaced by $V_{\text{HNNH}}(T)$ and $r_{\text{NNH}}(T)$, respectively. Moreover, $V_{\text{H0Hopping}}(T)$, $R_{\text{H0Hopping}}(T)$, γ_{Hopping}, and $n_{\text{Hopping}}(T)$ are replaced by the absolute value of the ideal Hall voltage ($V_{\text{H0NNH}}(T)$), the absolute value of the ideal Hall coefficient ($R_{\text{H0NNH}}(T)$), the Hall factor (γ_{NNH}), and the density of hopping charge carriers ($n_{\text{NNH}}(T)$) for NNH conduction, respectively. From Eqs. 11 and 12, $V_{\text{H0NNH}}(T)$ and $R_{\text{H0NNH}}(T)$ are respectively expressed as

$$V_{\text{H0NNH}}(T) = R_{\text{H0NNH}}(T)\frac{I_{\text{NNH}}B}{w} \tag{17}$$

and

$$R_{\text{H0NNH}}(T) = \frac{\gamma_{\text{NNH}}}{qn_{\text{NNH}}(T)}. \tag{18}$$

The existence probabilities of Al^- and Al^0 sites are $f_A(E_{Al})$ and $1 - f_A(E_{Al})$, respectively, where $f_A(E)$ is the Fermi–Dirac distribution function for acceptors and defined as

$$f_A(E) = \frac{1}{1 + g_A \exp\left(\frac{E - E_F}{k_B T}\right)}, \tag{19}$$

and g_A is the acceptor degeneracy factor. Because holes can hop from Al^0 sites to their nearest-neighbor Al^- sites and electrons can hop from Al^- sites to their nearest-neighbor Al^0 sites, $P_h(T)$ and $P_e(T)$ are replaced by $f_A(E_{Al})$ and $1 - f_A(E_{Al})$, respectively. Consequently, $V_{Hh}(T)$ and $V_{He}(T)$ are respectively expressed as

$$V_{Hh}(T) = V_{H0NNH}(T) f_A(E_{Al}) \tag{20}$$

and

$$V_{He}(T) = V_{H0NNH}(T) \left[1 - f_A(E_{Al})\right], \tag{21}$$

using Eqs. 14 and 15. $V_{HNNH}(T)$ can be derived using Eqs. 16, 20, and 21 as

$$V_{HNNH}(T) = V_{Hh}(T) - V_{He}(T) = V_{H0NNH}(T) \left[2 f_A(E_{Al}) - 1\right]. \tag{22}$$

Using Eqs. 8, 17, and 22, we obtain $R_{HNNH}(T)$ as

$$R_{HNNH}(T) = R_{H0NNH}(T) \left[2 f_A(E_{Al}) - 1\right], \tag{23}$$

indicating that $R_{HNNH}(T)$ is positive when $f_A(E_{Al}) > 0.5$ and negative when $f_A(E_{Al}) < 0.5$. In p-type semiconductors, in general, $R_{HNNH}(T)$ is negative at low temperatures because E_F is intermediate between E_{Al} and E_V; that is, $f_A(E_{Al}) < 0.5$. Consequently, in heavily Al-doped 4H-SiC, $R_H(T)$ becomes negative for NNH conduction.

Sign of $R_H(T)$ in VRH conduction. In VRH conduction, holes or electrons can hop to unoccupied localized states for energies between $E_F \pm \Delta E$ [19, 35]. As shown on the left side of Fig. 8(c), under $\mathcal{E}$ an electron hops from a localized state to a higher-energy localized state unoccupied by an electron (i.e., LS+h^+) or a hole hops from a localized state to a higher-energy localized state unoccupied by a hole (i.e., LS+e^-). The right side of Fig. 8(c) shows that under $\mathcal{E}$ an electron hops from a localized state to LS+h^+ with lower energy or a hole hops from a localized state to LS+e^- with lower energy.

In Fig. 8(e), $V_{HHopping}(T)$ and $r_{Hopping}(T)$ are replaced by $V_{HVRH}(T)$ and $r_{VRH}(T)$, respectively. Moreover, $V_{H0Hopping}(T)$, $R_{H0Hopping}(T)$, $\gamma_{Hopping}$, and $n_{Hopping}(T)$ are replaced by the absolute value of the ideal Hall voltage ($V_{H0VRH}(T)$), the absolute value of the ideal Hall coefficient ($R_{H0VRH}(T)$), the Hall factor (γ_{VRH}), and the density of hopping charge carriers ($n_{VRH}(T)$) for VRH conduction, respectively. From Eqs. 11 and 12, $V_{H0VRH}(T)$ and $R_{H0VRH}(T)$ are respectively expressed as

$$V_{H0VRH}(T) = R_{H0VRH}(T) \frac{I_{VRH} B}{w} \tag{24}$$

and

$$R_{H0VRH}(T) = \frac{\gamma_{VRH}}{q n_{VRH}}. \tag{25}$$

Under B, a large amount of holes at energy levels lower than E_F can easily hop to LS+e^- at energy levels higher than E_F; in addition, a large amount of electrons at energy levels higher than E_F can easily hop to LS+h^+ at energy levels lower than E_F. Therefore, the approximate hopping probabilities of holes ($P_{hVRH}(T)$) and electrons ($P_{eVRH}(T)$) under B can be defined as [19]

$$P_{hVRH}(T) \equiv \frac{\int_{E_F}^{E_F + \Delta E} g(\epsilon) f_{LS}(\epsilon) \mathrm{d}\epsilon}{N_{sum}(T)}, \tag{26}$$

and

$$P_{\mathrm{eVRH}}(T) \equiv \frac{\int_{E_\mathrm{F}-\Delta E}^{E_\mathrm{F}} g(\epsilon)\left[1-f_{\mathrm{LS}}(\epsilon)\right]\mathrm{d}\epsilon}{N_{\mathrm{sum}}(T)}, \tag{27}$$

with

$$N_{\mathrm{sum}}(T) \equiv \int_{E_\mathrm{F}}^{E_\mathrm{F}+\Delta E} g(\epsilon) f_{\mathrm{LS}}(\epsilon)\mathrm{d}\epsilon + \int_{E_\mathrm{F}-\Delta E}^{E_\mathrm{F}} g(\epsilon)\left[1-f_{\mathrm{LS}}(\epsilon)\right]\mathrm{d}\epsilon, \tag{28}$$

where ϵ is the energy and $f_{\mathrm{LS}}(\epsilon)$ is the Fermi–Dirac distribution function for the localized states.

In the case where $g(E)$ around E_F decreases with increasing E (e.g., the band tail above E_V), as shown in Fig 2(a),

$$\int_{E_\mathrm{F}}^{E_\mathrm{F}+\Delta E} g(\epsilon) f_{\mathrm{LS}}(\epsilon)\mathrm{d}\epsilon < \int_{E_\mathrm{F}-\Delta E}^{E_\mathrm{F}} g(\epsilon)\left[1-f_{\mathrm{LS}}(\epsilon)\right]\mathrm{d}\epsilon. \tag{29}$$

Therefore,

$$P_{\mathrm{hVRH}}(T) < P_{\mathrm{eVRH}}(T). \tag{30}$$

However, in the case where $g(E)$ around E_F increases with increasing E (e.g., the band tail below E_C),

$$P_{\mathrm{hVRH}}(T) > P_{\mathrm{eVRH}}(T). \tag{31}$$

Because $P_\mathrm{h}(T)$ and $P_\mathrm{e}(T)$ can be approximately replaced by $P_{\mathrm{hVRH}}(T)$ and $P_{\mathrm{eVRH}}(T)$, respectively, $V_{\mathrm{Hh}}(T)$ and $V_{\mathrm{He}}(T)$ in Fig. 8(e) can be described as

$$V_{\mathrm{Hh}}(T) \simeq V_{\mathrm{H0VRH}}(T) P_{\mathrm{hVRH}}(T) \tag{32}$$

and

$$V_{\mathrm{He}}(T) \simeq V_{\mathrm{H0VRH}}(T) P_{\mathrm{eVRH}}(T), \tag{33}$$

and we can then derive the expression for $V_{\mathrm{HVRH}}(T)$ as

$$V_{\mathrm{HVRH}}(T) = V_{\mathrm{Hh}}(T) - V_{\mathrm{He}}(T) \simeq V_{\mathrm{H0VRH}}(T)\left[2P_{\mathrm{hVRH}}(T)-1\right]. \tag{34}$$

Consequently, we obtain $R_{\mathrm{HVRH}}(T)$ as

$$R_{\mathrm{HVRH}}(T) \simeq R_{\mathrm{H0VRH}}(T)\left[2P_{\mathrm{hVRH}}(T)-1\right], \tag{35}$$

indicating that $R_{\mathrm{HVRH}}(T)$ becomes negative in the case where $P_{\mathrm{hVRH}}(T) < 0.5$ (e.g., the band tail above E_V) and positive in the case where $P_{\mathrm{hVRH}}(T) > 0.5$ (e.g., the band tail below E_C). In other words, $R_{\mathrm{HVRH}}(T)$ becomes negative in p-type semiconductors and positive in n-type semiconductors. Thus, our simple physical model can explain the sign reversal of $R_\mathrm{H}(T)$ in a-Si:H; that is, it can explain why negative and positive $R_\mathrm{H}(T)$ values were observed in p-type and n-type a-Si:H, respectively [29–31]. In the case of heavily Al-doped 4H-SiC, finally, we demonstrate that $R_\mathrm{H}(T)$ becomes negative for VRH conduction.

Net density of hopping charge carriers in NNH conduction. When the density of Al^0 (n_{Al^0}) is greater than the density of Al^- (n_{Al^-}), I_{NNH} is explained by the hopping of all of the electrons at Al^- sites to their nearest-neighbor Al^0 sites. From a different perspective, I_{NNH} can also be described by the hopping of a portion of the holes at Al^0, whose density is equal to n_{Al^-}, to their nearest-neighbor Al^- sites. These descriptions indicate that

$$n_{\mathrm{NNH}}(T) = n_{\mathrm{Al}^-} = N_{\mathrm{Al}} f_\mathrm{A}(E_{\mathrm{Al}}), \tag{36}$$

where N_{Al} is the density of Al acceptors, which is less than or equal to C_{Al}.

When n_{Al^0} is less than n_{Al^-}, by contrast, I_{NNH} can be explained by the hopping of all of the holes at Al^0 sites to their nearest-neighbor Al^- sites or by the hopping of a portion of the electrons at Al^- sites, whose density is equal to n_{Al^0}, to their nearest-neighbor Al^0 sites. Therefore,

$$n_{\mathrm{NNH}}(T) = n_{\mathrm{Al}^0} = N_{\mathrm{Al}} \left[1 - f_{\mathrm{A}}(E_{\mathrm{Al}})\right]. \tag{37}$$

In other words, at $f_{\mathrm{A}}(E_{\mathrm{Al}}) < 0.5$,

$$n_{\mathrm{NNH}}(T) = N_{\mathrm{Al}} f_{\mathrm{A}}(E_{\mathrm{Al}}), \tag{38}$$

and at $f_{\mathrm{A}}(E_{\mathrm{Al}}) > 0.5$,

$$n_{\mathrm{NNH}}(T) = N_{\mathrm{Al}} \left[1 - f_{\mathrm{A}}(E_{\mathrm{Al}})\right]. \tag{39}$$

Activation energies for NNH conduction. For NNH conduction, analogous to band conduction, $\rho_{\mathrm{NNH}}(T)$ can be defined as

$$\rho_{\mathrm{NNH}}(T) = \frac{1}{\sigma_{\mathrm{NNH}}(T)} \equiv \frac{1}{q n_{\mathrm{NNH}}(T) \mu_{\mathrm{NNH}}(T)}, \tag{40}$$

where $\sigma_{\mathrm{NNH}}(T)$ is the conductivity for NNH conduction and $\mu_{\mathrm{NNH}}(T)$ is the mobility of hopping charge carriers for NNH conduction.

The density of charge carriers determined by Hall effect measurements ($n_{\mathrm{HallNNH}}(T)$) is defined as

$$R_{\mathrm{HNNH}}(T) \equiv \frac{\gamma_{\mathrm{NNH}}}{q n_{\mathrm{HallNNH}}(T)}. \tag{41}$$

From Eqs. 12, 23, and 41, we obtain the relationship between $n_{\mathrm{HallNNH}}(T)$ and $n_{\mathrm{NNH}}(T)$ as

$$n_{\mathrm{HallNNH}}(T) = \frac{n_{\mathrm{NNH}}(T)}{2f(E_{\mathrm{Al}}) - 1}. \tag{42}$$

Here, negative and positive values of $n_{\mathrm{HallNNH}}(T)$ are regarded as the electron density and the hole density, respectively.

In heavily Al-doped 4H-SiC, because E_{F} at low temperatures is located between E_{Al} and E_{V} [36, 37],

$$f_{\mathrm{A}}(E_{\mathrm{Al}}) \simeq 0. \tag{43}$$

Thus, from Eqs. 18 and 23,

$$R_{\mathrm{HNNH}}(T) = R_{\mathrm{H0NNH}}(T) \left[2f(E_{\mathrm{Al}}) - 1\right] \simeq -R_{\mathrm{H0NNH}}(T) = -\frac{\gamma_{\mathrm{NNH}}}{q n_{\mathrm{NNH}}(T)}, \tag{44}$$

and from Eq. 19,

$$f_{\mathrm{A}}(E_{\mathrm{Al}}) = \frac{1}{1 + g_{\mathrm{A}} \exp\left(\dfrac{E_{\mathrm{Al}} - E_{\mathrm{F}}}{k_{\mathrm{B}} T}\right)} \simeq \frac{1}{g_{\mathrm{A}}} \exp\left(-\frac{E_{\mathrm{Al}} - E_{\mathrm{F}}}{k_{\mathrm{B}} T}\right), \tag{45}$$

indicating that, from Eq. 38,

$$n_{\mathrm{NNH}}(T) \simeq \frac{N_{\mathrm{Al}}}{g_{\mathrm{A}}} \exp\left(-\frac{E_{\mathrm{Al}} - E_{\mathrm{F}}}{k_{\mathrm{B}} T}\right). \tag{46}$$

Equations 40 and 44 respectively show that

$$\rho_{\mathrm{NNH}}(T) \simeq \frac{g_{\mathrm{A}}}{q N_{\mathrm{Al}} \mu_{\mathrm{NNH}}(T)} \exp\left(\frac{E_{\mathrm{Al}} - E_{\mathrm{F}}}{k_{\mathrm{B}} T}\right) \tag{47}$$

and

$$R_{\mathrm{HNNH}}(T) \simeq -\frac{\gamma_{\mathrm{NNH}} g_{\mathrm{A}}}{q N_{\mathrm{Al}}} \exp\left(\frac{E_{\mathrm{Al}} - E_{\mathrm{F}}}{k_{\mathrm{B}} T}\right). \tag{48}$$

Because E_{F} is weakly dependent on T at low temperatures [36, 37], the value of $E_{\mathrm{Al}} - E_{\mathrm{F}}$ in Eqs. 47 and 48 is nearly constant at low temperatures, indicating that

$$\Delta E_{\mathrm{RHNNH}} = E_{\mathrm{Al}} - E_{\mathrm{F}}. \tag{49}$$

However, $\mu_{\mathrm{NNH}}(T)$ results in a difference of the temperature dependences between Eqs. 47 and 48.

At $f_{\mathrm{A}}(E_{\mathrm{Al}}) < 0.5$, $\sigma_{\mathrm{NNH}}(T)$ in NNH conduction is proportional to (1) the density of hopping charge carriers (i.e., $n_{\mathrm{NNH}}(T)$); (2) the probability of Al acceptor sites being unoccupied by charge carriers at E_{Al} (i.e., $1 - f_{\mathrm{A}}(E_{\mathrm{Al}})$); (3) the wave function overlap of the two nearest-neighbor Al acceptor states, which can be expressed as $\exp(-2R_{\mathrm{Al}}/\alpha_0)$ [28], where R_{Al} is the average distance between nearest-neighbor Al acceptor sites and α_0 is the localization length of Al acceptors; and (4) the thermally assisted transfer rate over the difference in energy (W_{Al}) between two nearest-neighbor Al acceptor levels, which can be described as $\nu_{\mathrm{ph}} \exp(-W_{\mathrm{Al}}/k_{\mathrm{B}}T)$. Therefore,

$$\sigma_{\mathrm{NNH}}(T) \propto q n_{\mathrm{NNH}}(T) \left[1 - f_{\mathrm{A}}(E_{\mathrm{Al}})\right] \exp\left(-\frac{2R_{\mathrm{Al}}}{\alpha_0}\right) \nu_{\mathrm{ph}} \exp\left(-\frac{W_{\mathrm{Al}}}{k_{\mathrm{B}} T}\right). \tag{50}$$

From Eqs. 40 and 50,

$$\mu_{\mathrm{NNH}}(T) = C \left[1 - f_{\mathrm{A}}(E_{\mathrm{Al}})\right] \exp\left(-\frac{2R_{\mathrm{Al}}}{\alpha_0}\right) \nu_{\mathrm{ph}} \tag{51}$$

because $W_{\mathrm{Al}} \simeq 0$, where C is a proportional constant. Because $f_{\mathrm{A}}(E_{\mathrm{Al}}) \simeq 0$ at low temperatures,

$$\mu_{\mathrm{NNH}}(T) \simeq C \nu_{\mathrm{ph}} \exp\left(-\frac{2R_{\mathrm{Al}}}{\alpha_0}\right). \tag{52}$$

Compared with $n_{\mathrm{NNH}}(T)$, $\mu_{\mathrm{NNH}}(T)$ exhibits very weak temperature dependence, similar to the temperature dependence of ν_{ph}, indicating that

$$\Delta E_{\rho\mathrm{NNH}} \simeq E_{\mathrm{Al}} - E_{\mathrm{F}}. \tag{53}$$

Consequently, at low temperatures, the activation energy of $R_{\mathrm{H}}(T)$ is similar to that of $\rho(T)$. Furthermore, the value of $E_{\mathrm{Al}} - E_{\mathrm{F}}$ for the sample with a C_{Al} of 9.6×10^{19} cm^{-3} is approximately estimated as 32 meV from the slopes at low temperatures in Fig. 3.

Conclusions

We investigated $\rho(T)$ and $R_{\mathrm{H}}(T)$ for thick heavily Al-doped p-type 4H-SiC epilayers grown by CVD and determined the relationship between the conduction mechanisms and the values of T and C_{Al}, from which the resistivity in VRH conduction is found not to decrease with increasing C_{Al}.

We have also proposed a general physical model to explain negative $R_{\mathrm{H}}(T)$ at low temperatures in hopping conduction from the viewpoint of the hopping of electrons and holes, which is applicable to NNH and VRH conduction. In hopping conduction, electrons or holes are restricted to seeking unoccupied sites to which to hop, indicating that the sign of $R_{\mathrm{H}}(T)$ is determined by the difference between the density of hopping sites for holes and the density of hopping sites for electrons under an applied magnetic flux density. $R_{\mathrm{H}}(T)$ becomes negative when the occupation probability for electrons at E_{Al} is less than 0.5 in NNH conduction or when the localized-state density around E_{F} decreases with increasing E in VRH conduction.

In NNH conduction, the density of charge carriers determined by Hall effect measurements is found to be $n_{\mathrm{NNH}}(T)/(2f(E_{\mathrm{Al}})-1)$, where $n_{\mathrm{NNH}}(T)$ is the net density of hopping charge carriers from which the NNH current arises.

Furthermore, we have elucidated the reason why the activation energy of $R_{\mathrm{H}}(T)$ approaches that of $\rho(T)$ in NNH conduction and can estimate the approximate values of $E_{\mathrm{Al}}-E_{\mathrm{F}}$ from the activation energies of $\rho(T)$ and $R_{\mathrm{H}}(T)$ in NNH conduction.

Acknowledgments

This work was supported in part by JSPS KAKENHI Grant Number JP 20K04565, and the Council for Science, Technology and Innovation (CSTI), the Cross-ministerial Strategic Innovation Promotion Program (SIP), and the ”Next generation power electronics/Consistent R&D of next-generation SiC power electronics” project (funding agency: NEDO). The authors would like to thank S. Ji, K. Eto, Y. Ishida, K. Kojima, T. Kato, S. Yoshida, and H. Okumura at the National Institute of Advanced Industrial Science and Technology, Japan, for sample preparation and discussion, and T. Imamura, K. Takano, K. Okuda, K. Ogawa, K. Ozawa, K. Iida, T. Nishijima, M. Ogami, and Y. Kubota at the Matsuura Laboratory for measurements of resistivity and Hall coefficients.

References

[1] S.Y. Ji, K. Kojima, Y. Ishida, S. Saito, H. Yamaguchi, S. Yoshida, H. Tsuchida, and H. Okumura: Jpn. J. Appl. Phys. Vol. 54 (2015), p. 04DP08.

[2] S.Y. Ji, K. Kojima, Y. Ishida, S. Saito, T. Kato, H. Tsuchida, S. Yoshida, and H. Okumura: J. Crystal Growth Vol. 380 (2013), p. 85.

[3] K. Tone and J.H. Zhao, IEEE Trans. on Electron Devices Vol. 46 (1999), p. 612.

[4] J. Pernot, S. Contreras, and J. Camassel, J. Appl. Phys. Vol. 98 (2005), p. 023706.

[5] A. Parisini and R. Nipoti, J. Appl. Phys. Vol. 114 (2013), p. 243703.

[6] A. Parisini, M. Gorni, A. Nath, L. Belsito, M. V. Rao, and Nipoti, J. Appl. Phys. Vol. 118 (2015), p. 035101.

[7] A. Parisini, A. Parisini, and R. Nipoti, J. Phys.: Condens. Matter Vol. 29 (2017), p. 035703.

[8] A. Koizumi, J. Suda, and T. Kimoto, J. Appl. Phys. Vol. 106 (2009), p. 013716.

[9] C. Sylvie, K. Leszek, K. Pawel, A. Roxana, P. Hervé, C. Thierry, Z. Marcin, K. Maria, J. Sandrine, and Z. Konstantinos, Mater. Sci. Forum Vol. 858 (2016), p. 249.

[10] M. Krieger, K. Semmelroth, and G. Pensl, Mater. Sci. Forum Vol. 457-460 (2004), p. 685.

[11] M. Krieger, K. Semmelroth, H. B. Weber, G. Pensl, M. Rambach, and L. Frey, Mater. Sci. Forum Vol. 556-557 (2007), p. 367.

[12] S. Y. Ji, K. Eto, S. Yoshida, K. Kojima, Y. Ishida, S. Saito, H. Tsuchida, and H. Okumura, Appl. Phys. Express Vol. 8 (2015), p. 121302.

[13] H. Matsuura, A. Takeshita, T. Imamura, K. Takano, K. Okuda, A. Hidaka, S. Y. Ji, K. Eto, K. Kojima, T. Kato, S. Yoshida, and H. Okumura, Appl. Phys. Express Vol. 11 (2018), p. 101302.

[14] H. Matsuura, A. Takeshita, T. Imamura, K. Takano, K. Okuda, A. Hidaka, S.Y. Ji, K. Eto, K. Kojima, T. Kato, S. Yoshida, and H. Okumura, Mater. Sci. Forum Vol. 924 (2018), p. 188.

[15] H. Matsuura, A. Takeshita, T. Imamura, K. Takano, K. Okuda, A. Hidaka, S.Y. Ji, K. Eto, K. Kojima, T. Kato, S. Yoshida, and H. Okumura, Jpn. J. Appl. Phys. Vol. 58 (2019), p. 098004.

[16] H. Matsuura, R. Nishihata, A. Takeshita, T. Imamura, K. Takano, K. Okuda, A. Hidaka, S.Y. Ji, K. Eto, K. Kojima, T. Kato, S. Yoshida, and H. Okumura, Mater. Sci. Forum Vol. 963 (2019), p. 324.

[17] H. Matsuura, R. Nishihata, A. Takeshita, K. Ogawa, T. Imamura, K. Takano, K. Okuda, A. Hidaka, S.Y. Ji, K. Eto, K. Kojima, T. Kato, S. Yoshida, and H. Okumura, Mater. Sci. Forum Vol. 1004 (2020), p. 215.

[18] H. Matsuura, A. Takeshita, A. Hidaka, S.Y. Ji, K. Eto, T. Mitani, K. Kojima, T. Kato, S. Yoshida, and H. Okumura, Jpn. J. Appl. Phys. Vol. 59 (2020), p. 051004.

[19] H. Matsuura, Y. Kondo, K. Iida, A. Hidaka, S.Y. Ji, K. Eto, T. Mitani, K. Kojima, T. Kato, S. Yoshida, and H. Okumura, Jpn. J. Appl. Phys. Vol. 60 (2021), p. 031008.

[20] A. Hidaka, A. Takeshita, K. Ogawa, T. Imamura, K. Takano, K. Okuda, H. Matsuura, S.Y. Ji, K. Eto, T. Mitani, K. Kojima, T. Kato, S. Yoshida, and H. Okumura, Mater. Sci. Forum Vol. 1004 (2020), p. 224.

[21] M. Bezaquen, B. Belache, and D. Waksh, Phys. Rev. B Vol. 44 (1991), p. 13105.

[22] S.B. Mikhirin and K.F. Shtel'makh, Physica B Vol. 308-310 (2001), p. 881.

[23] B. Gunning, J. Lowder, M. Moseley, and W.A. Doolittle, Appl. Phys. Lett. Vol. 101 (2012), p. 082106.

[24] D. Emin, Phil. Mag. Vol. 35 (1977), p. 1189.

[25] M. Grunewald, P. Thomas, and D. Wurrtz, J. Phys. C Vol. 14 (1981), p. 4083.

[26] T. Holstein, Phys. Rev. Vol. 131 (1963), p. 2445.

[27] R. Németh and B. Mühlschlegel, Solid State Commun. Vol. 66 (1988), p. 999.

[28] R. A. Street, *Hydrogenated Amorphous Silicon* (Cambridge University Press, Cambridge, 1991).

[29] P.G. Le Comber, D. I. Jones, and W. E. Spear, Philos. Mag. Vol. 35 (1977), p. 1173.

[30] J. Dresner, Appl. Phys. Lett. Vol. 37 (1980), p. 742.

[31] H. Overhof, Philos. Mag. B Vol. 44 (1981), p. 317.

[32] C.E. Nebel, M. Rother, M. Stutzmann, C. Summonte, and M. Heintze, Philos. Mag. Lett. Vol. 74 (1996), p. 455.

[33] I. Crupi, S. Mirabella, D. D'Angelo, S. Gibilisco, A. Grasso, S. Di Marco, F. Simone, and A. Terrasi, J. APpl. Phys. Vol. 107 (2010), p. 043503.

[34] L. J. van der Pauw, Philips Res. Rep. Vol. 13 (1958), p. 1.

[35] B. I. Shklovskii and A. L. Efros, *Electronic Properties of Doped Semiconductors* (Springer-Verlag, Berlin, 1984).

[36] H. Matsuura, M. Komeda, S. Kagamihara, H. Iwata, R. Ishihara, T. Hatakeyama, T. Watanabe, K. Kojima, T. Shinohe, and K. Arai, J. Appl. Phys. Vol. 96 (2004), p. 2708.

[37] H. Matsuura, *Determination Methods of Densities and Energy Levels of Impurities and Defects Affecting Majority-Carrier Concentration in Next-Generation Semiconductor*, in Advanced in Condensed Matter and Materials Research Vol. 10, (Nova Science Publishers, Inc., 2011) Chap. 7.

[38] A. Avdonin, P. Skupiński, and K. Grasza, Physica B Vol. 483 (2016), p. 13.